

# Evidence for heteromorphic chromatin fibers from analysis of nucleosome interactions

Sergei A. Grigoryev<sup>a,1,2</sup>, Gaurav Arya<sup>b,1</sup>, Sarah Correll<sup>a</sup>, Christopher L. Woodcock<sup>c</sup>, and Tamar Schlick<sup>d,2</sup>

<sup>a</sup>Department of Biochemistry and Molecular Biology, Penn State University College of Medicine, H171, Milton S. Hershey Medical Center, P.O. Box 850, University Drive, Hershey, PA 17033; <sup>b</sup>Department of Nanoengineering, University of California at San Diego, 9500 Gilman Drive, La Jolla, CA 92093; <sup>c</sup>Biology Department, University of Massachusetts, Amherst, MA 01003; and <sup>d</sup>Department of Chemistry and Courant Institute of Mathematical Sciences, New York University, 251 Mercer Street, New York, NY 10012

Edited by Charles R. Cantor, Sequenom Inc., San Diego, CA, and approved June 18, 2009 (received for review March 27, 2009)

**The architecture of the chromatin fiber, which determines DNA accessibility for transcription and other template-directed biological processes, remains unknown. Here we investigate the internal organization of the 30-nm chromatin fiber, combining Monte Carlo simulations of nucleosome chain folding with EM-assisted nucleosome interaction capture (EMANIC). We show that at physiological concentrations of monovalent ions, linker histones lead to a tight 2-start zigzag dominated by interactions between alternate nucleosomes ( $i \pm 2$ ) and sealed by histone N-tails. Divalent ions further compact the fiber by promoting bending in some linker DNAs and hence raising sequential nucleosome interactions ( $i \pm 1$ ). Remarkably, both straight and bent linker DNA conformations are retained in the fully compact chromatin fiber as inferred from both EMANIC and modeling. This conformational variability is energetically favorable as it helps accommodate DNA crossings within the fiber axis. Our results thus show that the 2-start zigzag topology and the type of linker DNA bending that defines solenoid models may be simultaneously present in a structurally heteromorphic chromatin fiber with uniform 30 nm diameter. Our data also suggest that dynamic linker DNA bending by linker histones and divalent cations in vivo may mediate the transition between tight nucleosome packing within discrete 30-nm fibers and self-associated higher-order chromosomal forms.**

chromatin structure | electron microscopy | mesoscopic modeling | Monte Carlo simulations | linker histone

The DNA in eukaryotic chromatin is packed and functionally regulated by histones and nonhistone architectural proteins (1). The primary packing level is represented by an array of repeating units, the nucleosomes, where the DNA is wound around histone octamers (2). Further compaction is achieved through a hierarchy of folding levels, including the 30-nm chromatin fiber (secondary level) and more compact and self-associating tertiary and quaternary forms whose structures are unknown (3–6). Because DNA conformation in chromatin and nucleosome packing are intimately connected to DNA/protein recognition and gene regulation, there has been intense interest in understanding chromatin structure, energetics, and dynamics. Some experimental studies have suggested that nucleosomal arrays fold in a zigzag arrangement with relatively straight linkers and a 2-start nucleosome interaction pattern that brings each nucleosome in proximity to its second nearest neighbor (7–10) consistent with chromatin fibers observed in situ (11). Other evidence suggests that chromatin condensed with linker histones and divalent cations such as  $Mg^{2+}$  can form either zigzag structures with various nucleosome topologies (12, 13) or solenoid-like arrangements. The latter class of structures has bent DNA linkers and predominant interactions between either nearest neighbor nucleosomes (14, 15) and/or between every fifth or sixth nucleosome along the chain (16, 17).

The picture has become more complex recently with our heightened appreciation for the influence of structural details such as linker DNA length variability and the presence of linker histones on the resulting fiber architectures. For example, the Rhodes group showed that fiber compaction is both repeat length and linker-histone dependent (18). Analyses of known structures by the Rippe

group (19, 20) also suggested the large impact of nucleosome geometry on fiber compaction and the possible role of linker histones in converting between 2 fiber forms. Their systematic Monte Carlo simulations also support the notion that nucleosome interdigitation explains higher order chromatin structure and that the nucleosome repeat length affects the internal structure of the chromatin fiber. Other innovative modeling and simulation approaches for chromatin have explored various aspects of chromatin structure (21–25).

Here we examine by complementary innovative computational and experimental approaches the effect of linker histones and  $Mg^{2+}$  ions on the internal structure of physiologically compact chromatin. The modeling approach involves Monte Carlo simulations of a coarse-grained “mesoscale” chromatin model that accounts for important structural and energetic components whereas still making oligonucleosome simulations computationally feasible (26–29). Because experimental observations emphasize the polymorphic and irregular nature of chromatin fiber in vitro and in vivo—stemming from linker DNA flexibility, rotational flexibility of DNA in the nucleosome core, and flexible histone tails that interact with the DNA and counterions within as well as between the nucleosomes (11, 30)—our mesoscale modeling approach uniquely takes into account histone-tail flexibility, linker-histone electrostatics and orientation,  $Mg^{2+}$ -induced electrostatic screening, and linker-DNA bending at physiological conditions, as well as thermal fluctuations and entropic effects. A summary of the model and extensive applications to monovalent salt-dependent folding/unfolding dynamics and energetics and histone tail effects are provided in the *SI Text*; see also (31). The experimental technique EM-assisted nucleosome interaction capture (EMANIC) uses formaldehyde cross-linking to fix a limited number of internucleosome contacts in the condensed state, after which the chromatin is decondensed at low salt, and transmission EM is applied to provide a quantitative assessment of nucleosome-to-nucleosome contacts. Formaldehyde cross-links protein-protein and protein-DNA interactions within 2 Å and may involve the side-chain nitrogens of histones and the exocyclic amino and the endocyclic imino groups of DNA (32). It thus allows us to probe chromatin structure without preliminary chemical modification and without a bias for site-specific nucleosome interactions.

The modeling and experimental approaches presented here produce remarkably similar results that lead us to suggest a detailed mechanism by which linker histone and  $Mg^{2+}$  combine to establish the internal organization of a chromatin fiber. Compared with

Author contributions: S.A.G., G.A., and T.S. designed research; S.A.G., G.A., and S.C. performed research; C.L.W. contributed new reagents/analytic tools; S.A.G., G.A., S.C., C.L.W., and T.S. analyzed data; and S.A.G., G.A., and T.S. wrote the paper.

The authors declare no conflict of interest.

This article is a PNAS Direct Submission.

<sup>1</sup>S.A.G. and G.A. contributed equally to this work.

<sup>2</sup>To whom correspondence may be addressed. E-mail: sag17@psu.edu or schlick@nyu.edu.

This article contains supporting information online at [www.pnas.org/cgi/content/full/0903280106/DCSupplemental](http://www.pnas.org/cgi/content/full/0903280106/DCSupplemental).

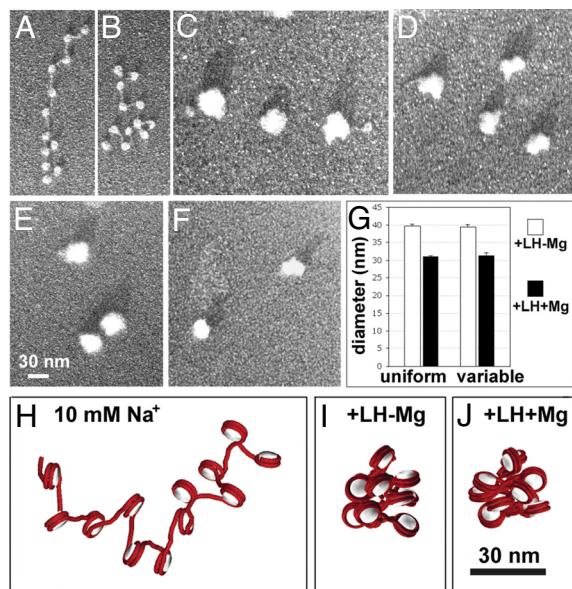


**Fig. 1.** Electron microscopy and modeling of unfolded and compact 12-nucleosome arrays. (A–F) Electron micrographs (platinum shadowing) of regular  $207 \times 12$  core arrays in 5 mM NaCl (A and B), regular LH-arrays condensed in 150 mM NaCl (C) and 1 mM MgCl<sub>2</sub> (D), and variable LH-arrays condensed in 150 mM NaCl (E) or 1 mM MgCl<sub>2</sub> (F). (G) Average diameter of uniform and variable LH-arrays condensed in 150 mM NaCl (white columns) and 1 mM MgCl<sub>2</sub> (black columns). Error bars represent standard errors of mean. (H–J) Models of representative  $12 \times 207$  oligonucleosomes at 0.01 M monovalent salt without LH (H), and 0.15 M monovalent salt with LH (I), and with LH and Mg<sup>2+</sup> (J) highlight compaction effects of linker histones and Mg<sup>2+</sup>.

oligonucleosome species with neither linker histones nor divalent ions (–LH–Mg), oligonucleosomes with linker histones (+LH–Mg) constrict the linker-DNA entry-exit angle and tighten a 2-start zigzag arrangement of nucleosomes; with both linker histones and divalent ions (+LH+Mg), the increased electrostatic screening promotes linker DNA bending and their enhanced packing within the chromatin fiber. The resulting nucleosome interaction pattern—predominantly 2-start zigzag interspersed by interactions between nearest-neighbor nucleosomes via bent DNA—also suggests that the increased bending of linker DNA initially promotes compact and rigid longitudinal packing of the 30-nm fiber within the 2-start zigzag architecture and may lead to higher-order forms that underlie the condensed heterochromatin of terminally differentiated cells and metaphase chromosomes.

## Results

**Experimental and Modeling Analysis of Nucleosome Array Compaction.** Nucleosome arrays of 12 residues with 207 bp repeats that mimic the nucleosome repeat in chicken erythrocytes have been widely used in multiple biochemical and biophysical studies (see e.g., 30, 33, 34). Our 12-nucleosome arrays featuring the nucleosome positioning sequence of clone 601 DNA (35) contained linker DNA with either uniform ( $207 \times 12$ ) or varied lengths in a fixed pattern  $(205 - 207 - 209) \times 4$ , thus mimicking the natural variation in nucleosome repeat length of  $\pm 2$  bp (36, 37). The nucleosome positions and complete saturation of the nucleosome templates by histone cores were confirmed by micrococcal nuclease mapping (Fig. S1) and EM (Fig. 1 A and B and Fig. S2 a and b). Both the uniform and variable –LH–Mg, +LH–Mg, and +LH+Mg nucleosome arrays produce similar compaction at 150 mM NaCl or 1 mM MgCl<sub>2</sub> and similar sedimentation velocities at low salt (10 mM Na<sup>+</sup>) and as determined by EM (Fig. 1 C–G) and sedimentation (Table 1 and Fig. S2). Thus, the widely accepted experimental values (60S sedimentation, 1.5 mM Mg<sup>2+</sup> self-association point) for

**Table 1. Chromatin compaction assessment by sedimentation coefficients of  $207 \times 12$  oligonucleosomes with and without linker histones and Mg<sup>2+</sup> ions**

Array Type	Monovalent salt (M)	Computed $S_{20,w}$ (S)	Experimental $S_{20,w}$ (S)*	Computed packing ratio (nuc/11 nm)
Without LH and Mg <sup>2+</sup> (–LH–Mg)	0.01	$30.0 \pm 0.1$	29.8	2.5
With LH, without Mg <sup>2+</sup> (+LH–Mg)	0.01	$44.3 \pm 0.7$	37.0	4.0
With LH and Mg <sup>2+</sup> (+LH+Mg)	0.15	$48.8 \pm 1.7$	55.6	7.0
With LH and Mg <sup>2+</sup> (+LH + Mg)	0.15	$53.5 \pm 2.2$	60.0* 56.0†	8.2

\*Sedimentation at 10 mM Na<sup>+</sup> and 1 mM Mg<sup>2+</sup>.

†Sedimentation at 150 mM Na<sup>+</sup> and 1 mM Mg<sup>2+</sup>.

12-unit arrays (33, 34, 38) are reproduced. In addition, sedimentation experiments with  $207 \times 12$  LH-containing arrays in the presence of 1 mM Mg<sup>2+</sup> and 150 mM Na<sup>+</sup> (as also explored in mesoscopic modeling) show lower sedimentation values of the main peak (56S) than in 1 mM Mg<sup>2+</sup> and 10 mM Na<sup>+</sup> (Fig. S2g and Table 1) consistent with the finding that 1 mM Mg<sup>2+</sup> and linker histone are sufficient to induce the most compact chromatin folding (33, 38).

Mesoscopic modeling of the same 3 species of  $207 \times 12$  oligonucleosomes (Fig. 1 H–J) reveals a striking resemblance to the oligonucleosome diameters and shapes observed by EM. The calculated sedimentation values from the ensemble average using the Kirkwood-Bloomfield formulation (28, 39) and fiber packing ratios (Table 1) further underscore the dramatic effect of LH and Mg<sup>2+</sup> on the condensation of chromatin. LH alone causes significant compaction of oligonucleosomes at low monovalent salt (from 30S to 44S and from 2.5 to 3.5 nucleosomes/11 nm of fiber) and physiological salt (from 39S to 49S and from 4.0 to 7.0 nucleosomes/11 nm). Mg<sup>2+</sup> causes further compaction of the oligonucleosomes (to 53.5S and 8.2 nucleosomes/11 nm).

Overall, good agreement is obtained between the modeling and sedimentation experiments for –LH–Mg arrays and +LH–Mg arrays at low salt; at physiological salt, the changes predicted by modeling for +LH–Mg arrays are in qualitative agreement with experiments (Table 1). The somewhat smaller compaction values than  $\sim 10$  nucleosomes/11 nm previously reported for chromatin fibers with similar DNA linker length by EM of Mg<sup>2+</sup>-compacted chromatin (17) and computational modeling (13, 19) are likely because of sampling limitations and neglected internucleosomal interactions [e.g., hydrogen bonding between histone surfaces (40)]. Both our approaches, however, yield a similar (5S) increase in sedimentation constant with Mg<sup>2+</sup> ions. More generally, in silico and in vitro experiments confirm that linker histone and divalent cations are both required for maximal packing of nucleosome arrays with repeat lengths typical of higher eukaryotes (16, 31). For short linker DNA, the requirement for condensation may be different because Mg<sup>2+</sup> ions alone lead to dramatic compaction. This was found by modeling and EMANIC investigations of  $167 \times 12$  chromatin systems: Corresponding –LH–Mg arrays displayed a dramatically stronger Mg<sup>2+</sup>-dependent compaction relative to  $207 \times 12$  systems in terms of sedimentation (52S vs. 37S; Fig. S2) and overall shape. This is consistent with recent observations of Routh et al. (18) that arrays with long linkers (207 bp) but not those with short linkers (167 bp) require both linker histone and Mg<sup>2+</sup> for complete condensation.

**Internucleosomal Interactions Patterns from Modeling.** Modeling can directly measure internucleosomal interactions from the simulated configurations by accounting for the strength of tail-mediated

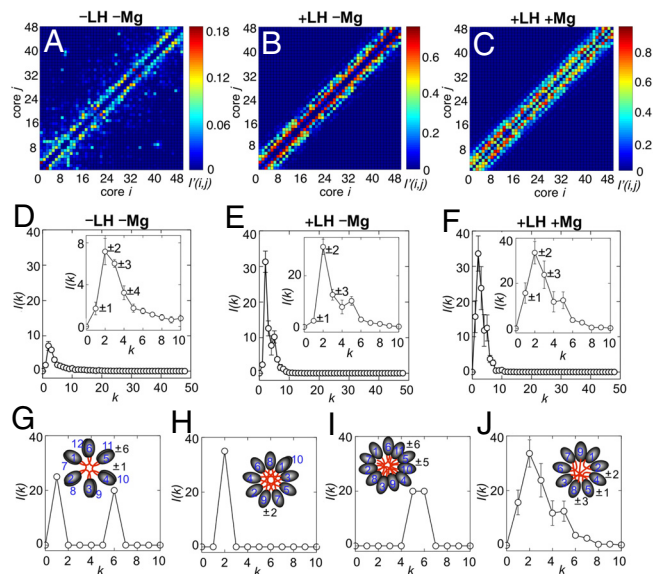


**Fig. 2.** Internucleosomal interaction pattern predicted for distinct chromatin 30-nm fiber models. (A–C) Interaction-intensity matrices at 0.15 M monovalent salt without LH and  $Mg^{2+}$  (A), with LH and without  $Mg^{2+}$  (B), and with both LH and  $Mg^{2+}$  (C) show the intensity of the tail-mediated interactions between nucleosome core  $i$  and  $j$  matrix [ $I'(i, j)$ ]. (D–F) The associated plots decompose the dominant neighboring interactions,  $I(k)$ , where  $k$  is the nucleosome separator. Interactions at  $k = 1, 2,$  and  $3$  nucleosomes are indicated as  $\pm 1, \pm 2,$  and  $\pm 3$ , correspondingly. (G–J) reference internucleosomal interaction patterns corresponding to the 3 existing models of nucleosome arrangement: (G) solenoid model (14), (H) 2-start zigzag model (10), and (I) interdigitated nucleosome model (17) compared with that obtained from our Monte Carlo simulations for +LH+Mg chromatin (J).

interactions between nucleosome cores  $i$  and  $j$  along the chromatin chain (29). The interaction-intensity matrices  $I'(i, j)$  (Fig. 2 A–C) describe the fraction of time (configurations) that nucleosome pairs interact with one another (i.e., approach within 80% of Van der Waals radii) through all interactions involving the histone tails; the associated plots further decompose these interactions into  $i \pm k$  neighbors (Fig. 2 D–F). The patterns obtained for the 3 species of oligonucleosomes predict how the fiber morphology changes upon the addition of LH and  $Mg^{2+}$  and allow comparison with experimental findings and other published models. In the classic 6-nucleosome-per-turn solenoid model (14), nucleosome interactions are predicted to involve mostly  $i \pm 1$  and  $i \pm 6$ ; for 2-start zigzag-based structures (9, 10) dominant interactions are at  $i \pm 2$ ; and for interdigitated solenoid models (16, 17) strongest interactions at  $i \pm 5$  or  $i \pm 6$  are predicted (Fig. 2 G–J). Our modeling predicts that without LH and  $Mg^{2+}$ , the fiber is extended and  $i \pm 2$  interactions dominate, as expected for 2-start zigzag arrangements, whereas  $i \pm 3$  interactions are weaker (Fig. 2 A and D). Adding LH enhances the zigzag folding, promotes dominant  $i \pm 2$  interactions and increases other short-ranged interactions, up to  $i \pm 6$  (Fig. 2 B and E). The enhanced  $i \pm 2$  interactions reflect the substantial LH-induced compaction, bringing alternate nucleosomes closer together as in zigzag structures (Fig. 2H); this enhancement of short-range internucleosomal interactions stiffens the fiber and eliminates the long-range interactions present without LH (cf. Fig. 2 A and B). Importantly, Monte Carlo simulations of +LH–Mg chromatin converge to the same zigzag structure when started from 4 different oligonucleosome configurations (2 variants of zigzag and 2 different solenoid structures; Fig. S3).

Adding  $Mg^{2+}$  to LH-compacted chromatin fiber model leaves the  $i \pm 2$  interactions dominant but raises nearest-neighbor ( $i \pm 1$ ) and  $i \pm 3$  interactions (Fig. 2 C and F), suggesting linker DNA bending (Fig. 2J). The interaction pattern also becomes more

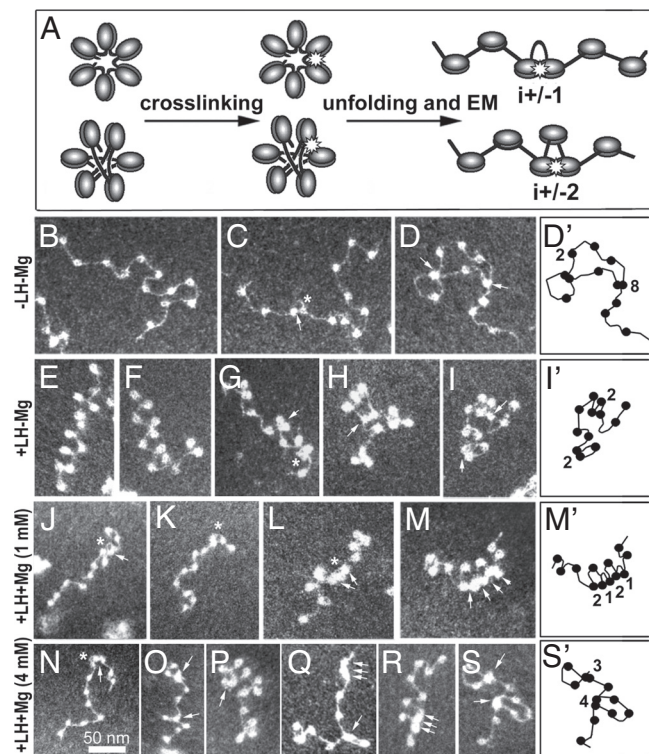


**Fig. 3.** EMANIC analysis of internucleosomal interactions. (A) Scheme of the EMANIC procedure. The 2 models for the structure of the chromatin 30-nm fiber, namely solenoid (Top) and zigzag (Bottom), lead to dominant  $i \pm 1$  and  $i \pm 2$  internucleosome interactions, respectively. (B–S) Capturing internucleosomal interactions after limited formaldehyde cross-linking. EM of nucleosome reconstitutes showing uniform core arrays (B and D), variable core array (C), uniform LH-containing arrays (E, F, I–O, Q–S), and variable LH-containing arrays (G, H, P). Cross-linking was performed in 5 mM NaCl (B, C, E–G), 150 mM NaCl (D, H, I), 1 mM  $MgCl_2$  (J–M), and 4 mM  $MgCl_2$  (panels N–S). Arrows show nucleosome interactions, and asterisks indicate interacting nearest-neighbor nucleosomes connected by a short DNA loop. D', I', M', and S' diagram the nucleosome arrays corresponding to the respective EM images.

intense at the main diagonal and the fiber stiffens, also consistent with other experiments (30). For the +LH+Mg species, results represent averages of 2 main ensembles (see *SI Text*).

Our modeling also predicts an average internucleosomal interaction energy of  $-1.9$  kcal/mol per interacting nucleosome pair, computed as the average electrostatic contribution from ensemble histone tail/nonparent nucleosome interactions only. However, this value cannot be directly compared with energies extracted from force-extension measurements of LH-inclusive chromatin in monovalent salt [ $-2$  kcal/mol (41) and high salt ( $-8$  kcal/mol) in high Mg (15) conditions (2 mM  $Mg^{2+}$ )] that account for additional interactions and dissipative effects not counted and treated in our mesoscale model.

**Internucleosomal Interactions Mapping by EMANIC.** Partial formaldehyde cross-linking of nucleosomes interacting in condensed chromatin (Fig. 3A) with subsequent EM imaging (Fig. 3 B–S) provides an empirical evaluation of the internucleosome patterns. When –LH–Mg arrays are cross-linked in the unfolded state at 5 mM NaCl or at 150 mM NaCl (Fig. 4A) there are no significant changes in the number of loops ( $i \pm >1$ ) from the noncross-linked control. In contrast, cross-linking in the presence of 1 or 4 mM  $MgCl_2$  significantly ( $P < 0.005$ ) increases the proportion of  $i \pm 2$  interactions (Fig. 4B), consistent with the dominant 2-start zigzag topologies of chromatin fibers compacted by  $Mg^{2+}$  in the absence of linker histones (9).

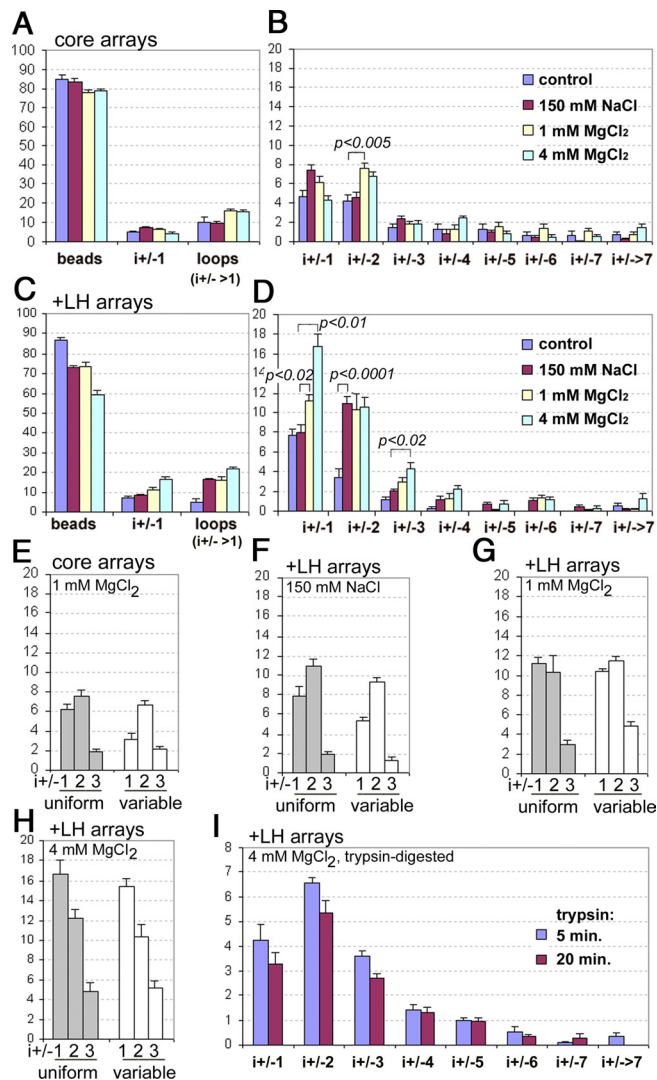


**Fig. 4.** Internucleosomal interactions in regular and variable nucleosomal arrays. (A–D) Internucleosomal interactions within reconstituted core nucleosome arrays (A and B) and LH-arrays (C and D) scored either without cross-linking (control) or after formaldehyde-cross-linking in the presence of 150 mM NaCl, 1 mM MgCl<sub>2</sub>, and 4 mM MgCl<sub>2</sub>. Histograms A and C show % total nucleosomes involved in no interactions (free beads), nearest neighbor ( $i \pm 1$ ), and loops ( $i \pm 2$  and more). Histograms B and D show % total nucleosomes involved in particular type of interaction. Student's *t* test *P* values for significant differences between the data sets are shown over the brackets. (E–H) % total nucleosomes from uniform (207 × 12) and variable (205 - 207 - 209) × 4 core (E) and LH-arrays (F–H) involved in nearest neighbor interactions ( $i \pm 1$ ) and 2 most prominent types of loops ( $i \pm 2$  and  $i \pm 3$ ). The reconstituted arrays were cross-linked by formaldehyde at 150 mM NaCl, 1 mM MgCl<sub>2</sub>, or 4 mM MgCl<sub>2</sub> as indicated. (I) Internucleosomal interactions detected after formaldehyde-cross-linking in the presence of 4 mM MgCl<sub>2</sub> and 5 min or 20 min digestion with 1 μg/mL trypsin as indicated.

Without cross-linking, +LH–Mg arrays show a significantly smaller number of loops than –LH–Mg arrays (Fig. 4C), demonstrating that linker histone itself does not promote loop formation. However, when cross-linked at 150 mM NaCl, the +LH–Mg arrays produce a significant ( $P < 10^{-4}$ ) 3.2-fold increase in  $i \pm 2$  interactions (Fig. 4D), consistent with a 2-start zigzag arrangement of nucleosome cores as predicted by modeling (Fig. 5).

When +LH+Mg (1 mM Mg<sup>2+</sup>) arrays are cross-linked, the relative frequency of  $i \pm 2$  is similar to that in NaCl-condensed chromatin, but there is a significant ( $P < 0.02$ ) 1.4-fold increase in the proportion of  $i \pm 1$  interactions over the noncross-linked level

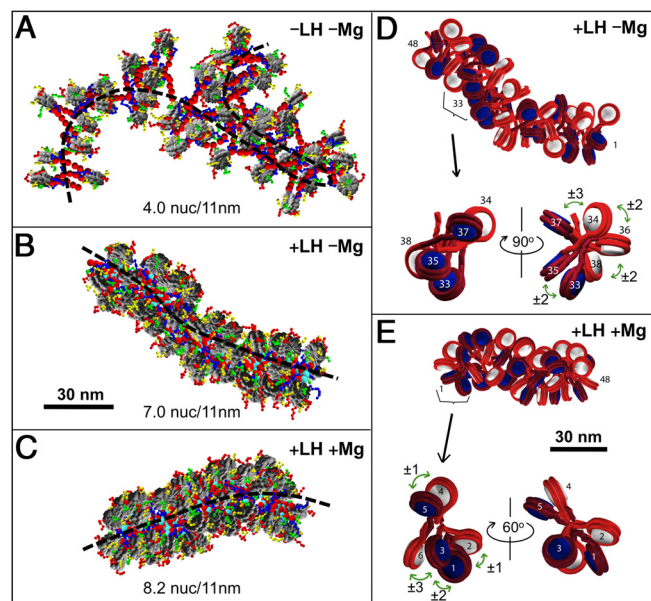


**Fig. 5.** Effect of linker histone and divalent cation on chromatin fiber compaction and associated linker DNA configurations. (A–C) Coarse-grained chromatin models of representative 48-unit oligonucleosomes at 0.15 M monovalent salt without LH (A), with LH (B), and with LH and Mg<sup>2+</sup> (C) highlight compaction and fiber stiffening effects of linker histones as shown by the fiber axes geometry (dashed black lines). Nucleosome cores are shown by gray disks, linker DNA by large red spheres, linker histone by turquoise spheres, and individual core-histone tails are colored by yellow (H2A), red (H2B), blue (H3), and green (H4). (D and E) Space-filling models based on MC simulation of 48-unit oligonucleosome chains compacted at 0.15 M monovalent salt with LH (D), and with LH and Mg<sup>2+</sup> (E). (D) Compaction at 150 mM NaCl leads to a 2-start zigzag chromatin fiber with predominantly  $i \pm 2$  interactions between the most proximal nucleosomes (33 and 35, 34 and 36, 36 and 38) shown by green arrows. (E) In the presence of 1 mM MgCl<sub>2</sub>, several nucleosomes have bent linkers resulting in  $i \pm 1$  interactions (nucleosomes 1 and 2, 4 and 5), interspersed with  $i \pm 2$  (1 and 3) and  $i \pm 3$  (6 and 3) interactions. Odd-numbered nucleosomes are indicated by burgundy for the DNA and blue for the cores. Even-numbered nucleosomes are indicated by red for the DNA and white for the cores.

(Fig. 4D). EM (Fig. 3J–M) also shows that  $i \pm 1$  and  $i \pm 2$  interactions are interspersed within single +LH+Mg arrays. This is consistent with increased structural heterogeneity of nucleosome linkers and their propensity to bend in the presence of Mg<sup>2+</sup> ion as predicted by the modeling (Fig. 2J). An additional EMANIC experiment with LH-arrays in the presence of 1 mM Mg<sup>2+</sup> plus 150 mM Na<sup>+</sup> showed a very similar pattern of nucleosome interactions confirming promotion of  $i \pm 1$  interactions by Mg<sup>2+</sup> (Fig. S4A).

To account for possible longer-ranged interactions that could be missing from the relatively short 12-unit arrays, we also conducted EMANIC experiments with 24-unit nucleosome arrays. The unfolded 24-unit arrays showed a significantly increased number of long-range nucleosome loops under EM in a good agreement with the increased cross-fiber interactions in long (Fig. 5A) vs. short (Fig. 1H) arrays, as also predicted by modeling. The increased length and conformational flexibility hindered precise detection of all 24 nucleosomes in most cases. Nevertheless, the apparent loop sizes resolved for 24-unit nucleosomes reveal the same pattern of interactions as in 12-unit systems (Fig. S4B).

Variable (205 - 207 - 209) × 4 oligonucleosome arrays show very similar cross-linking patterns to uniform arrays for all salt conditions tested (Fig. 4E–H) with significant increases both in  $i \pm 1$  ( $P < 2 \times 10^{-5}$ ) and  $i \pm 3$  ( $P < 2 \times 10^{-3}$ ) in 1 mM MgCl<sub>2</sub> compared with NaCl-condensed chromatin. Thus, for both regular and variable arrays our data support a chromatin fiber structure with predominant interactions between alternate nucleosomes along a 2-start

zigzag path ( $i \pm 2$ ) that becomes interspersed with  $i \pm 1$  and  $i \pm 3$  contacts in the presence of both linker histones and divalent ions.

**Probing Tertiary Chromatin Structure by EMANIC.** With increased  $Mg^{2+}$  concentration, nucleosomal arrays undergo reversible self-association (42) attributed to the formation of global tertiary chromatin structures (4). When +LH+Mg arrays are cross-linked at 4 mM  $MgCl_2$  (where the material was completely self-associated: Fig. S4C), unfolded in a low-salt buffer, and then examined by EM, a dramatic increase in the proportions of both  $i \pm 1$  interactions ( $\sim 2.1$ -fold,  $P < 0.01$ ) and  $i \pm 3$  loops (2.4-fold,  $P < 0.02$ ) compared with NaCl-condensed chromatin is seen (Fig. 4D). This occurs with both uniform and variable arrays (Fig. 4H).

To distinguish short-range nucleosome interactions from those that might originate from extended histone tail contacts, after nucleosome interactions have been fixed by formaldehyde in the condensed state, we conducted a controlled trypsin digestion of the nucleosomes (43) to cut N-terminal histone tails (Fig. S4D) while preserving the globular histone domains and the primary nucleosome core structure. As with intact chromatin, we observe nucleosome loops (Fig. S4E) with nucleosome interaction patterns dominated by  $i \pm 1$ ,  $i \pm 2$ , and  $i \pm 3$  but with the proportion of  $i \pm 1$  reduced as compared with intact chromatin (Fig. 4I). The overall nucleosome interaction patterns are remarkably similar to modeling predictions for +LH+Mg chromatin (Fig. 2F), further supporting the dominance of the 3 short-range internucleosome interactions ( $i \pm 1$ ,  $i \pm 2$ , and  $i \pm 3$ ) both in condensed and self-associated chromatin fibers.

**Chromatin Fiber Configuration from Modeling.** Representative oligonucleosome models from the -LH-Mg, +LH-Mg, and +LH+Mg ensembles, each including 48 nucleosomes (Fig. 5), illustrate the dramatic compaction trend upon addition of LH and  $Mg^{2+}$  and the roles of each constituent in compacting chromatin. Without LH and  $Mg^{2+}$ , an irregular zigzag fiber of width  $< 30$  nm with straight linker DNA forms, with frequent sharp turns (Fig. 5A). Two distinct conformations for the linker DNAs are obtained: Crossed conformations where linker DNAs intersect after emerging from the nucleosome, and open conformations where they diverge from each other, also consistent with experiments (44, 45). The 2 types of linker DNA trajectories are better assessed from their positional distribution plots (projected onto the nucleosomal and dyad planes; Fig. S5) and from the twin-peaked distribution of the angles formed by 3 consecutive nucleosomes (in Fig. S6).

Specifically, modeling suggests that LH compacts chromatin drastically, from 4 to 7 nucleosomes/11 nm (Table 1) and increases fiber stiffness (as detected by the simulation ensemble fluctuation range) whereas eliminating sharp bends in the fiber (Fig. 5B). The positional distribution of the linkers becomes narrower (Fig. S5 c and d) with a prominent peak at  $39^\circ$  (Fig. S6b). The resulting, more regular structure shows a zigzag fiber with straight linker DNAs and predominant  $i \pm 2$  interactions (Fig. 5D) compacted in an accordion-like manner consistent with AFM and cryo-EM observations (8, 23).

As expected, divalent ions and LH cooperate to further compact the fiber (Fig. 5C) consistent with EM observations (17); see also Fig. 1. This compaction is characterized by a fiber architecture with mostly straight zigzag features, but with an emerging small population of bent linker DNAs leading to increased  $i \pm 1$  and  $i \pm 3$  interactions (Fig. 5E). Perhaps contrary to intuition, this conformational heterogeneity promotes, rather than inhibits, chromatin fiber compaction. These features can be characterized by the widening of the linker DNA trajectory distribution (Fig. S5 e and f) and the biphasic distribution of the triplet angle  $\theta$  resulting from bent and straight linker DNA; the  $39^\circ$  peak associated with the pure zigzag is decreased, and the broad peak between  $60$ – $120^\circ$  appears, associated with bent linker DNA (Fig. S6b). However, despite this broad conformational variation, the resulting

nucleosome chain folds into an energetically stable fiber with uniform diameter of 31–33 nm consistent with the diameters and extended stiff conformations of long chromatin fibers revealed by ultrastructural analysis in vitro and in situ (11, 17, 23). Thus, our modeling and experimental approaches both converge to reveal a principle of chromatin fiber organization that reconciles the 2-start zigzag topology with linker DNA bending in one heteromorphic chromatin fiber structure.

## Discussion and Conclusions

Our work provides evidence, by both modeling and experiment, of a heteromorphic chromatin fiber with both straight and bent linker DNA in the presence of linker histones and divalent ions for typical repeat lengths. Linker histones alter the trajectory of linker DNAs to promote greater interactions between alternate nucleosomes; divalent ions induce bending of a portion of linker DNAs, effectively reducing the number of linker DNA crossings at the chromatin axis; and internucleosomal interactions may laterally stabilize a compact state of chromatin, causing the chromatin fibers to become more compact and stiff. The increased fiber stiffness has the potential to inhibit communication between gene regulatory regions that form chromatin loops for active transcription (46) and is consistent with the recent structural analysis of the 16-kb heterochromatin region separating the differentially regulated FOA and  $\beta$ -globin genes (47). The fibers in the presence of divalent ions are predicted to contain  $\sim 20\%$  bent linker DNAs, bringing some consecutive nucleosomes closer. This value was obtained from modeling by measuring the average angle between the exiting linker DNA trajectory of 1 nucleosome and the entering linker DNA trajectory of the next nucleosome and taking the fraction with bending angle  $> 90^\circ$  (see Fig. S6D); note that a perfect zigzag would yield an average angle of  $0^\circ$ , whereas a pure solenoid with 6 nucleosomes per term corresponds to  $120^\circ$ . This suggests that the  $Mg^{2+}$ -induced reduction in persistence length of linker DNAs introduces attractive internucleosomal interactions, due in large part to histone tail contacts [strength 3–4  $k_B T$ , where  $k_B$  is the Boltzmann constant and  $T$  is the temperature (31)], offsetting the energy of linker DNA bending. Higher concentrations of  $Mg^{2+}$  (2 mM and above) are shown to strengthen internucleosomal interactions and have been suggested to reinforce the nearest-neighbor contacts in the chromatin fibers forced to unfold by magnetic tweezers (15). In unconstrained fibers, however, such  $Mg^{2+}$  concentrations lead to extensive self-association (34). This, however, does not eliminate the mixed straight/bent linker conformation as it is supported by simultaneous presence of  $i \pm 1$  and  $i \pm 2$  interactions in chromatin fibers condensed by 4 mM  $Mg^{2+}$ . The resulting oligonucleosomes with mostly straight but some bent linker DNAs reconcile apparently contradictory evidence for straight (7–10) or bent (48, 49) linker DNA conformations. Such heteromorphic fibers (with straight/bent linker DNA configurations) allow chromatin to achieve higher levels of compaction, because bent linker DNAs require fewer linker DNA crossings in the middle of the fiber and hence reduce electrostatic repulsion between DNA molecules. This fiber structure may also more easily accommodate local conformational variations of the nucleosome fiber resulting from the dynamic wrapping/unwrapping of nucleosomal DNA (6, 50), rotational flexibility of nucleosomal DNA (2), and short periods of linker histone association/dissociation on linker DNA (51).

Our modeling predicts a larger average electrostatic energy per  $i \pm 1$  interaction ( $-0.27$  kcal/mol) than for  $i \pm 2$  ( $-0.63$  kcal/mol). Consistent with previous notions that altered internucleosomal interactions could promote inter-fiber self-association (34, 52), a hypothetical scheme on Fig. S7 suggests how the bent linkers may destabilize  $i \pm 1$  interactions in *cis* (within fibers) and promote nucleosome interactions in *trans* (between fibers). Internucleosomal interactions in *trans* may account for partially interdigitated 30-nm fibers in the interphase nucleus (11) and for global chromatin condensation in metaphase chromosomes where divalent cation

levels are sharply increased (53) and no distinct 30 nm fibers are observed (54).

Future development of our modeling and EMANIC approaches could illuminate other aspects of native chromatin organization and suggest specific agents or protein factors capable of locking nucleosome arrays in active or silent configurations.

## Methods

**Mesoscale Modeling.** Full details of the model, validation studies, and applications are described in *SI Text*.

**Oligonucleosome Arrays.** Nucleosome 12-mer arrays were constructed using nucleosome core-positioning sequence from the original clone 601 DNA (35) and reconstituted with chicken erythrocyte core and linker histone H5 essentially as described (38). For more details of reconstitution, biochemical characterization, and ultracentrifugation of the reconstituted arrays see *SI Text*.

**Formaldehyde Cross-Linking.** Reconstituted nucleosomes (with and without histone H5) were prepared in 20- $\mu$ L aliquots with DNA concentration 50  $\mu$ g/mL in 10 mM HEPES, pH 7.5, 5 mM NaCl, and 0.1 mM EDTA. Some nucleosome aliquots were mixed either with 0.15 M NaCl (concentration of the 5 M stock solution was

verified by refractometry, cat# S7653; Sigma) or 1 or 4 mM  $MgCl_2$  (prepared from  $1 \pm 0.01$  M stock solution, cat# M1028; Sigma) and incubated for 15 min on ice and for 5 min at room temperature. A solution of 37% formaldehyde (ACS reagent; Fisher) was added to make samples contain 0.08% formaldehyde, and the samples were incubated for 5' at room temperature. An equal volume of the same reaction media (without formaldehyde) containing 100 mM glycine, pH 7.8, was added to quench the reaction, and the samples were dialyzed for 5 h against 10 mM Na-borate, pH 9.0, 0.1 mM EDTA to induce chromatin decondensation.

**Electron Microscopy.** Transmission EM of nucleosome arrays was conducted in dark-field mode. For more details of electron microscopy, data collection, and analysis, see *Experimental Procedures* in *SI Text*.

**ACKNOWLEDGMENTS.** We thank N. Chandra for providing the structure of the rat H1d linker histone; J. Widom for clone 601 DNA; M. Fried and M. Lopez for advice on analytical ultracentrifugation; E. Popova and N. Facompre for experimental assistance; and O. Perisic for providing images for Figs. 1 and 5. This work was supported by National Science Foundation Grants MCB-0615536 (to S.A.G.) and MCB-0316771 and National Institutes of Health Grant R01 GM55164 (to T.S.). Acknowledgment is also made to the donors of the American Chemical Society (Award PRF39225-AC4) Petroleum Research Fund and to Philip Morris USA and Philip Morris International for partial support of this research to T.S.

- Felsenfeld G, Groudine M (2003) Controlling the double helix. *Nature* 421:448–453.
- Richmond TJ, Davey CA (2003) The structure of DNA in the nucleosome core. *Nature* 423:145–150.
- Woodcock CL, Dimitrov S (2001) Higher order structure of chromatin and chromosomes. *Curr Opin Genet Dev* 11:130–135.
- Luger K, Hansen JC (2005) Nucleosome and chromatin fiber dynamics. *Curr Opin Struct Biol* 15:188–196.
- Tremethick DJ (2007) Higher-order structures of chromatin: The elusive 30 nm fiber. *Cell* 128:651–654.
- van Holde K, Zlatanova J (2007) Chromatin fiber structure: Where is the problem now? *Semin Cell Dev Biol* 18:651–658.
- Woodcock CL, Frado LL, Rattner JB (1984) The higher-order structure of chromatin: Evidence for a helical ribbon arrangement. *J Cell Biol* 99:42–52.
- Leuba SH, et al. (1994) Three-dimensional structure of extended chromatin fibers as revealed by tapping-mode scanning force microscopy. *Proc Natl Acad Sci USA* 91:11621–11625.
- Dorigo B, et al. (2004) Nucleosome arrays reveal the two-start organization of the chromatin fiber. *Science* 306:1571–1573.
- Schalch T, Duda S, Sargent DF, Richmond TJ (2005) X-ray structure of a tetranucleosome and its implications for the chromatin fibre. *Nature* 436:138–141.
- Horowitz RA, Agard DA, Sedat JW, Woodcock CL (1994) The three-dimensional architecture of chromatin in situ: Electron tomography reveals fibers composed of a continuously variable zig-zag nucleosomal ribbon. *J Cell Biol* 125:1–10.
- Williams SP, et al. (1986) Chromatin fibers are left-handed double helices with diameter and mass per unit length that depend on linker length. *Biophys J* 49:233–248.
- Wong H, Victor JM, Mozziconacci J (2007) An all-atom model of the chromatin fiber containing linker histones reveals a versatile structure tuned by the nucleosomal repeat length. *PLoS ONE* 2:e877.
- Thoma F, Koller T, Klug A (1979) Involvement of histone H1 in the organization of the nucleosome and of the salt-dependent superstructures of chromatin. *J Cell Biol* 83:403–427.
- Kruihof M, et al. (2009) Single-molecule force spectroscopy reveals a highly compliant helical folding for the 30-nm chromatin fiber. *Nat Struct Mol Biol* 16:534–540.
- Daban JR (2000) Physical constraints in the condensation of eukaryotic chromosomes. Local concentration of DNA versus linear packing ratio in higher order chromatin structures. *Biochemistry* 39:3861–3866.
- Robinson PJ, Fairall L, Huynh VA, Rhodes D (2006) EM measurements define the dimensions of the “30-nm” chromatin fiber: Evidence for a compact, interdigitated structure. *Proc Natl Acad Sci USA* 103:6506–6511.
- Routh A, Sandin S, Rhodes D (2008) Nucleosome repeat length and linker histone stoichiometry determine chromatin fiber structure. *Proc Natl Acad Sci USA* 105:8872–8877.
- Kepper N, Foethke D, Stehr R, Wedemann G, Rippe K (2008) Nucleosome geometry and internucleosomal interactions control the chromatin fiber conformation. *Biophys J* 95:3692–3705.
- Stehr R, Kepper N, Rippe K, Wedemann G (2008) The effect of internucleosomal interaction on folding of the chromatin fiber. *Biophys J* 95:3677–3691.
- Schiessel H, Gelbart WM, Bruinsma R (2001) DNA folding: Structural and mechanical properties of the two-angle model for chromatin. *Biophys J* 80:1940–1956.
- Wedemann G, Langowski J (2002) Computer simulation of the 30-nanometer chromatin fiber. *Biophys J* 82:2847–2859.
- Bednar J, et al. (1998) Nucleosomes, linker DNA, and linker histone form a unique structural motif that directs the higher-order folding and compaction of chromatin. *Proc Natl Acad Sci USA* 95:14173–14178.
- Mergell B, Everaers R, Schiessel H (2004) Nucleosome interactions in chromatin: Fiber stiffening and hairpin formation. *Phys Rev E Stat Nonlin Soft Matter Phys* 70:011915.
- Katritch V, Bustamante C, Olson WK (2000) Pulling chromatin fibers: Computer simulations of direct physical micromanipulations. *J Mol Biol* 295:29–40.
- Beard DA, Schlick T (2001) Computational modeling predicts the structure and dynamics of chromatin fiber. *Structure* 9:105–114.
- Sun J, Zhang Q, Schlick T (2005) Electrostatic mechanism of nucleosomal array folding revealed by computer simulation. *Proc Natl Acad Sci USA* 102:8180–8185.
- Arya G, Zhang Q, Schlick T (2006) Flexible histone tails in a new mesoscopic oligonucleosome model. *Biophys J* 91:133–150.
- Arya G, Schlick T (2006) Role of histone tails in chromatin folding revealed by a mesoscopic oligonucleosome model. *Proc Natl Acad Sci USA* 103:16236–16241.
- Kan PY, Lu X, Hansen JC, Hayes JC (2007) The H3 tail domain participates in multiple interactions during folding and self-association of nucleosome arrays. *Mol Cell Biol* 27:2084–2091.
- Arya G, Schlick T (2009) A tale of tails: How histone tails mediate chromatin compaction in different salt and linker histone environments. *J Phys Chem A* 113:4045–4059.
- Jackson V (1999) Formaldehyde cross-linking for studying nucleosomal dynamics. *Methods* 17:125–139.
- Carruthers LM, Bednar J, Woodcock CL, Hansen JC (1998) Linker histones stabilize the intrinsic salt-dependent folding of nucleosomal arrays: Mechanistic ramifications for higher-order chromatin folding. *Biochemistry* 37:14776–14787.
- Gordon F, Luger K, Hansen JC (2005) The core histone N-terminal tail domains function independently and additively during salt-dependent oligomerization of nucleosomal arrays. *J Biol Chem* 280:33701–33706.
- Lowary PT, Widom J (1998) New DNA sequence rules for high affinity binding to histone octamer and sequence-directed nucleosome positioning. *JMB* 276:19–42.
- Widom J (1992) A relationship between the helical twist of DNA and the ordered positioning of nucleosomes in all eukaryotic cells. *Proc Natl Acad Sci USA* 89:1095–1099.
- Woodcock CL, Grigoryev SA, Horowitz RA, Whitaker N (1993) A chromatin folding model that incorporates linker variability generates fibers resembling the native structures. *Proc Natl Acad Sci USA* 90:9021–9025.
- Huynh VA, Robinson PJ, Rhodes D (2005) A method for the in vitro reconstitution of a defined “30 nm” chromatin fibre containing stoichiometric amounts of the linker histone. *J Mol Biol* 345:957–968.
- Bloomfield V, Dalton WO, Van Holde KE (1967) Frictional coefficients of multisubunit structures. I. Theory. *Biopolymers* 5:135–148.
- Luger K, Mader AW, Richmond RK, Sargent DF, Richmond TJ (1997) Crystal structure of the nucleosome core particle at 2.8 Å resolution. *Nature* 389:251–260.
- Cui Y, Bustamante C (2000) Pulling a single chromatin fiber reveals the forces that maintain its higher-order structure. *Proc Natl Acad Sci USA* 97:127–132.
- Schwarz PM, Felthaus A, Fletcher TM, Hansen JC (1996) Reversible oligonucleosome self-association: Dependence on divalent cations and core histone tail domains. *Biochemistry* 35:4009–4015.
- Crane-Robinson C, Bohm L (1985) Structural studies of chromatin by using proteases. *Biochem Soc Trans* 13:303–306.
- Keper JF, et al. (2003) Conformation of reconstituted mononucleosomes and effect of linker histone H1 binding studied by scanning force microscopy. *Biophys J* 85:4012–4022.
- Toth K, Brun N, Langowski J (2006) Chromatin compaction at the mononucleosome level. *Biochemistry* 45:1591–1598.
- Rubtsov MA, Polikanov YS, Bondarenko VA, Wang YH, Studitsky VM (2006) Chromatin structure can strongly facilitate enhancer action over a distance. *Proc Natl Acad Sci USA* 103:17690–17695.
- Ghirlando R, Felsenfeld G (2008) Hydrodynamic studies on defined heterochromatin fragments support a 30-nm fiber having six nucleosomes per turn. *J Mol Biol* 376:1417–1425.
- Yao J, Lowary PT, Widom J (1991) Linker DNA bending induced by the core histones of chromatin. *Biochemistry* 30:8408–8414.
- Butler P, Thomas J (1998) Dinucleosomes show compaction by ionic strength consistent with binding to linker DNA. *JMB* 281:401–407.
- Poirier MG, Bussiek M, Langowski J, Widom J (2008) Spontaneous access to DNA target sites in folded chromatin fibers. *J Mol Biol* 379:772–786.
- Brown DT, Izard T, Misteli T (2006) Mapping the interaction surface of linker histone H1(0) with the nucleosome of native chromatin in vivo. *Nat Struct Mol Biol* 13:250–255.
- Grigoryev SA (2004) Keeping fingers crossed: Heterochromatin spreading through interdigitation of nucleosome arrays. *FEBS Lett* 564:4–8.
- Strick R, Strissel PL, Gavrilov K, Levi-Setti R (2001) Cation-chromatin binding as shown by ion microscopy is essential for the structural integrity of chromosomes. *J Cell Biol* 155:899–910.
- Eltsov M, MacLellan KM, Maeshima K, Frangakis AS, Dubochet J (2008) Analysis of cryo-electron microscopy images does not support the existence of 30-nm chromatin fibers in mitotic chromosomes in situ. *Proc Natl Acad Sci USA* 105:19732–19737.